49. Resonances

Revised August 2019 by D.M. Asner (BNL), C. Hanhart (Jülich) and E. Klempt (Bonn U.).

49.1 General Considerations

Perturbative methods can be applied to systems of quarks and gluons only for large momentum transfers (see review on 'Quantum Chromodynamics') and, under certain conditions, to some properties of systems that contain heavy quarks or very large momentum scales (see review on "Heavy-Quark and Soft-Collinear Effective Theory"). Dealing with Quantum Chromodynamics (QCD) in the low momentum transfer region is a very complicated, non-perturbative problem. The physical states appear as poles of the S–matrix either on physical sheet (bound states) or on the unphysical sheets (resonances) and manifest themselves as structures in experimental observables.

Resonances can show up either in so-called formation experiments, typically of the kind

$$A + B \rightarrow \mathbf{R} \rightarrow C_1 + ... + C_n \ ,$$

where they become visible in an energy scan (a perfect example of this being the R–function measured in e^+e^- annihilations — *cf.* the corresponding plots in the review on "Plots of Cross Sections and Related Quantities"), or together with a spectator particle S in production experiments of the kind

$$A + B \rightarrow \mathbf{R} + S \rightarrow [C_1 + ... + C_n] + S \ ,$$
$$Z \rightarrow \mathbf{R} + S \rightarrow [C_1 + ... + C_n] + S \ .$$

where the first reaction corresponds to an associated production, the second is a decay (see "Review of Multibody Charm Analyses"). In the latter case the resonance properties are commonly extracted from a Dalitz plot analysis (see review on "Kinematics") or projections thereof.

Resonance phenomena are very rich: while typical hadronic widths are of the order of 100 MeV (*e.g.*, for the meson resonances $\rho(770)$ or $\psi(4040)$ or the baryon resonance $\Delta(1232)$) corresponding to a lifetime of 10^{-23} s, the widths can also be as small as a few MeV (*e.g.* of $\phi(1020)$ or J/ψ) or as large as several hundred MeV (*e.g.* of the meson resonances $f_0(500)$ or $D_1(2430)$ or the baryon resonance $N(2190)$).

Typically, a resonance appears as a peak in the total cross section. If the structure is narrow and if there are no relevant thresholds or other resonances nearby, the resonance properties may be extracted employing a standard Breit-Wigner parameterization, if necessary improved by using an energy-dependent width (*cf.* Sec. 49.3.1 of this review). However, in general, unitarity and analyticity call for the use of more refined tools. When there are overlapping resonances with the same quantum numbers, the resonance terms should not simply be added but combined in a non–trivial way either in a K–matrix approximation (*cf.* Sec. 49.3.2 of this review) or using other advanced methods (*cf.* Sec. 49.3.6 of this review). Additional constraints from the S-matrix allow one to build more reliable amplitudes and in turn to reduce the systematic uncertainties of the resonance parameters: pole locations and residues. In addition, for broad resonances there is no direct relation anymore between pole location and the total width/lifetime — then the pole residues need to be used in order to quantify the decay properties.

For simplicity, throughout this review the formulas are given for distinguishable, scalar particles. The additional complications that appear in the presence of spins can be controlled in the helicity framework developed by Jacob and Wick [1], or in a non-covariant [2] or covariant [3] tensor operator formalism. Within these approaches, sequential (cascade) decays are commonly treated

as a coherent sum of two-body interactions. Most of the expressions below are given for two–body kinematics.
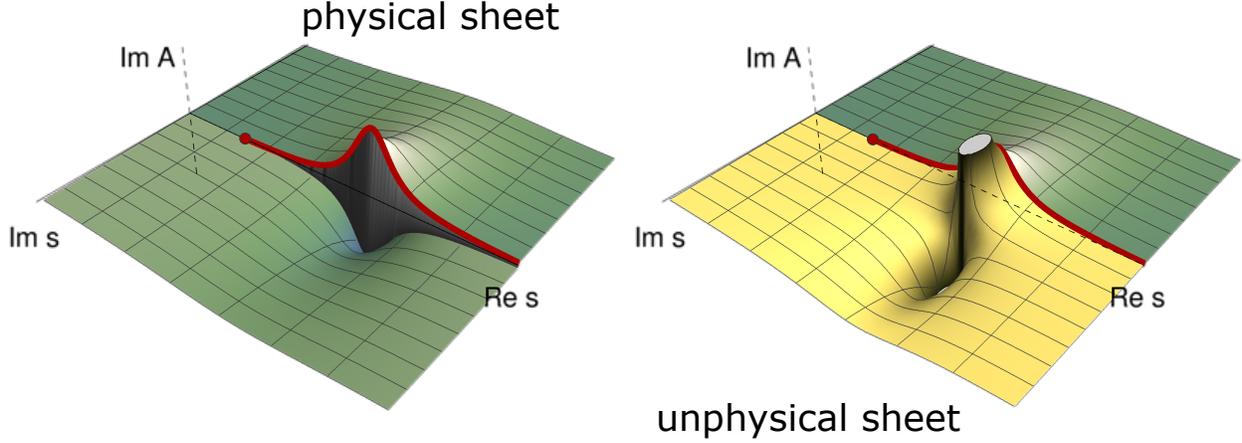

Figure 49.1: Imaginary part of a typical single–channel scattering amplitude with an isolated resonance. The solid red line shows the physical range of the Mandelstam variable s: It is real valued and starts from threshold shown by the red dot. The left plot shows the imaginary part of the amplitude in the complex S–plane that corresponds to the first physical sheet (green surface). The right plot shows analytic continuation of the same amplitude to the lower plane of the unphysical sheet (yellow surface). The latter contains the resonance pole. The two sheets are connected smoothly along the real axis above the threshold.

49.1.1 *Properties of the S-matrix*

The unitary operator that connects asymptotic *in* and *out* states is called the S–matrix. The scattering amplitude is defined as the interacting part of the S matrix. For the case of two interacting particles, it reads: (*cf.* Eq. (8) of the review on "Kinematics" but note: we here use a different sign convention as well as a different normalisation of the fields to be consistent with most books on field theory)

$$i(2\pi)^4\delta^4(p_1 + p_2 - p_1' - p_2')\,\mathcal{M}(p_1, p_2; p_1, p_2')_{ba} = {}_{\text{out}}\langle p_1'p_2', b|\,S - 1\,|p_1p_2, a\rangle_{\text{in}} \qquad (49.1)$$

where $|p_1p_2, a\rangle$ and $|p_1'p_2', b\rangle$ are asymptotic states of two non-interacting particles with momentum p_1, p_2 and p_1', p_2'. The channel labels a and b are multi–indices specifying all additional properties of the channel. In general, $\mathcal{M}$ is a matrix in channel space. For single particle states we employ the common relativistic normalization,

$$\langle p'|p\rangle = (2\pi)^3 2E_p\,\delta^3(\vec{p}\,' - \vec{p}), \qquad (49.2)$$

with $E_p = \sqrt{\vec{p}\,^2 + m^2}$. The scattering amplitude an analytic function of the Mandelstam variables s, t and u up to poles and kinematic singularities. Branch points appear whenever there is a channel opening — at each two-particle threshold the number of Riemann sheets doubles. Triangle topologies can induce logarithmic singularities on the unphysical sheets often called triangle singularities (TS) [4–6]. Analyticity and unitarity principles of the S-matrix put strong constraints to the function $\mathcal{M}(s,t)$. Poles refer either to bound states or to resonances. The former poles are located on the physical sheet, the latter are located on unphysical sheets. Naturally those located on the unphysical sheet closest to the physical one, often called the second sheet, have usually the largest impact on observables. Moreover, as follows from analyticity, if there is a pole at some

complex value of s, there must be another pole at its complex conjugate value, s^*. The pole with a negative imaginary part is closer to the physical axis and thus influences the observables in the vicinity of the resonance region more strongly (see Fig. 49.1). However, at the threshold both poles are always equally important. If there are resonances in subsystems of multi–particle states, branch points appear in the complex plane of the unphysical sheet(s) [6]. Any of these singularities can lead to some structure in the observables (see also Ref. [7]). If certain kinematical constraints are met, especially the TS can mimic resonance signals, as claimed in Refs. [8–13] or could in certain channels lead to significant shifts of resonance signals [14]. For a partial-wave-projected amplitude (see Sec. 49.1.3) additional singularities not related to resonance physics may emerge as a result of the partial-wave projection [15].

Further constraints come, *e.g.*, from crossing symmetry and duality [16]. Approaches based on analyticity and crossing symmetry, implemented via dispersion theory, like the Roy equations [17] or variants thereof, were developed and applied to $\pi\pi \to \pi\pi$ scattering [18–20], πK scattering [21], $\gamma\gamma \to \pi\pi$ [22] as well as pion-nucleon scattering [23].

49.1.2 *Consequences from unitarity*

In what follows, scattering amplitudes $\mathcal{M}$ and production amplitudes $\mathcal{A}$ will be distinguished, since unitarity puts different constraints on these. For the production amplitudes we require that the initial state is weakly coupled and, hence, the probability of the time-reversed reaction is negligibly small compared to the other coupled channels.

The discontinuity of the scattering amplitude over the unitarity cut is constrained by unitarity [24] to

$$\text{Disc}\,\mathcal{M}_{ba} = [\mathcal{M}_{ba} - \mathcal{M}_{ab}^*] = i\,(2\pi)^4 \sum_c \int d\Phi_c \mathcal{M}_{cb}^* \mathcal{M}_{ca}\ , \tag{49.3}$$

with Φ_c being the invariant phase space for channel c. The sum includes only open channels, *i.e.* those for which the production threshold is below the energy of the scattered system. Using time-reversal symmetry, and $\text{Disc}\,\mathcal{M}(s,t) = 2i\,\text{Im}(\mathcal{M}(s+i\epsilon,t))$ for the s-channel, the optical theorem follows

$$\text{Im}\,\mathcal{M}_{aa}(s,0) = 2q_a\sqrt{s}\,\sigma_{\text{tot}}(a \to \text{anything}), \tag{49.4}$$

where q_a denotes the relative momentum of the particles of channel a (see Eq. (17) of the review on "Kinematics"). The value $t = 0$ in Eq. (49.4) corresponds to forward scattering.

The unitarity relation for a production amplitude for a channel a is given by

$$[\mathcal{A}_a - \mathcal{A}_a^*] = i\,(2\pi)^4 \sum_c \int d\Phi_c \mathcal{M}_{ca}^* \mathcal{A}_c\ . \tag{49.5}$$

One application of the two-body-unitarity constraint from Eq. (49.5) is studies of the three-body decays in the Khuri-Treiman framework [25]. The standard procedure here is to derive the equations for the production amplitude for small values of the mass of the decaying particle in the scattering domain and relate it to the decay kinematics by an analytic continuation in the decay mass. Note that in this kinematics the connection between imaginary part and discontinuity employed to derive Eq. (49.4) no longer holds. The method was successfully applied to various decays of light mesons, $\eta \to 3\pi$ in Refs. [26–28], $\phi/\omega \to 3\pi$ in Ref. [29, 30], $\eta' \to \eta\pi\pi$ in Ref. [31], as well as to the charm-mesons decays $D^+ \to K^{0/-}\pi^{0/+}\pi^+$ [32, 33].

49.1.3 *Partial-wave decomposition*

It is often convenient to expand the scattering amplitude in partial waves. Since resonances have a well-defined spin, in the s-channel they appear only in the corresponding partial waves. For
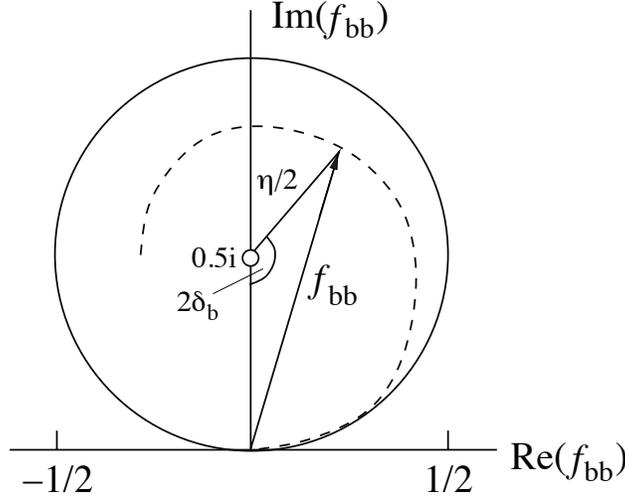
Figure 49.2: Argand plot showing a diagonal element of a partial-wave amplitude, a_{bb}, as a function of energy. The amplitude leaves the unitary circle (solid line) as soon as inelasticity sets in, $\eta < 1$ (dashed line).

scalar particles only one may write

$$\mathcal{M}_{ba}(s,t) = \sum_{j=0}^{\infty} (2j+1)\mathcal{M}_{ba}^{j}(s)P_j(\cos(\theta)) \ , \tag{49.6}$$

where j denotes the total angular momentum. For scalar particles it coincides with the orbital angular momentum of the particle pairs in the initial and the final state. To simplify notations we will drop the label j for the single-argument function $\mathcal{M}_{ba}(s)$. The unitarity constraint for $\mathcal{M}_{ba}(s)$ reads,

$$\operatorname{Im}\mathcal{M}_{ba} = \sum_{c} \mathcal{M}_{cb}^{*}\,\rho_c\,\mathcal{M}_{ca} \tag{49.7}$$

with ρ_c being a factor that is related to the two-body phase space in Eq. (12) of the review on "Kinematics",

$$\rho_c(s) = \frac{(2\pi)^4}{2}\int \mathrm{d}\Phi_2 = \frac{1}{16\pi}\frac{2|\vec{q}_c|}{\sqrt{s}}. \tag{49.8}$$

The partial-wave amplitudes $f_{ba}(s)$ are connected to $\mathcal{M}_{ba}(s)$ via

$$f_{ba}(s) = \sqrt{\rho_b}\,\mathcal{M}_{ba}(s)\,\sqrt{\rho_a} \ . \tag{49.9}$$

From this definition it follows for the unitarity condition that $\operatorname{Im} f_{ba}^{-1} = -\delta_{ba}$. Moreover, $\mathbb{I} + 2if$ is a unitary matrix. Hence, it can be parameterized as,

$$f_{bb} = (\eta_b \exp(2i\delta_b) - 1)/2i \ , \tag{49.10}$$

where δ_b denotes the phase shift for the scattering from channel b to channel b, η_b is elasticity parameter — also called inelasticity. One has $0 \leq \eta_b \leq 1$, where $\eta_b = 1$ refers to purely elastic scattering. The evolution with energy of a partial-wave amplitude f_{bb} can be displayed as a trajectory in an Argand plot, as shown in Fig. 49.2. In case of a two–channel problem, $\eta_b = \eta_a = \eta$, and the off–diagonal element is $f_{ba} = \sqrt{1 - \eta^2}/2 \, \exp(i(\delta_b + \delta_a))$.

The partial-wave-projected production amplitude $\mathcal{A}(s)$ (the label j is dropped for consistency) is also constrained by unitarity. From Eq. (49.5) follows,

$$\operatorname{Im}\mathcal{A}_a = \sum_b \mathcal{M}_{ab}^* \rho_b \mathcal{A}_b , \tag{49.11}$$

where the sum runs over all open channels. For purely elastic scattering, where the sum collapses to just the channel a, the Watson theorem, stating that the phase of $\mathcal{A}_a$ agrees with that of $\mathcal{M}_{aa}$, follows straightforwardly, since the left-hand side of Eq. (49.11) is a real number.

49.2 Properties of resonances

The main characteristics of a resonance is its pole position, s_R, in the complex s–plane that is independent of the reaction studied. The more traditional parameters mass M_R and total width Γ_R may be introduced via the pole parameters

$$\sqrt{s_R} = M_R - i\Gamma_R/2 . \tag{49.12}$$

Note that the standard Breit-Wigner parameters M_{BW} and Γ_{BW}, also introduced below, in general deviate from the pole parameters, *e.g.*, due to finite width effects and the influence of thresholds.

In addition to the pole location a resonance is characterized also by its residues that quantify its couplings to the various channels and allow one to define branching ratios. In the Meson Particle Listings the two-photon width of $f_0(500)$ is defined in terms of the corresponding residue. The Baryon Particle Listings give the elastic pole residues and normalized transition residues. However, different conventions are used in the two sectors, which are shortly outlined here.

In the close vicinity of the resonance pole the scattering matrix $\mathcal{M}$ can be written as

$$\lim_{s \to s_R} (s - s_R)\mathcal{M}_{ba} = -\mathcal{R}_{ba} . \tag{49.13}$$

The residues may be calculated via an integration along a closed contour around the pole using

$$\mathcal{R}_{ba} = -\frac{1}{2\pi i} \oint ds \mathcal{M}_{ba} . \tag{49.14}$$

The factorization of the residue $(\mathcal{R}_{ba})^2 = \mathcal{R}_{aa} \times \mathcal{R}_{bb}$ allows one to introduce pole couplings according to

$$\tilde{g}_a = \mathcal{R}_{ba}/\sqrt{\mathcal{R}_{bb}} . \tag{49.15}$$

The pole couplings are the only quantities that characterize the transition strength of a given resonance to some channel a independently of how the particular resonance was produced. One may define a partial width and a branching fraction even for a broad resonance via

$$\Gamma_{R \to a} = \frac{|\tilde{g}_a|^2}{M_R} \rho_a(M_R^2) \quad \text{and} \quad Br_a = \Gamma_{R \to a}/\Gamma_R , \tag{49.16}$$

where M_R and Γ_R were introduced in Eq. (49.12). This expression was used to define a two–photon width for the broad $f_0(500)$ (also called σ) [34, 35]. Eq. (49.16) defines a partial-decay width independent of the reaction used to extract the parameters. For a narrow resonance it maps smoothly onto the other common definition of the branching fraction, discussed in Eq. (49.22).

In the baryon sector it is common to define the residue with respect to the partial-wave amplitudes $f_{ba}(s)$ defined in Eq. (49.9) and with respect to $\sqrt{s}$ instead of s. Accordingly in the baryon listings the elastic pole residue, which refers to $\pi N \to \pi N$ scattering, is related to the residues introduced above via

$$r_{\pi N,\pi N} = \frac{\rho_{\pi N}(s_R)}{\sqrt{4s_R}} \mathcal{R}_{\pi N,\pi N} , \tag{49.17}$$

where the phase-space factor is to be evaluated at the pole.

49.3 Common parameterizations

Up to a few exceptions where sophisticated dispersive methods can be used or one restricts oneself to a very small energy range, there is in general no universal model-independent recipe to build the scattering amplitude. The resonance parameters extracted should not depend on the approach used, however, assuming that the amplitude fits relevant data of sufficient quality well. Deviations of resonance parameters obtained in different models which equally-well describe the data must be attributed to the systematic theory uncertainties.

49.3.1 *The Breit–Wigner paramerization*

First we focus on the most common case of resonances that appear in production reactions and consider the simplest approximation that is only appropriate for a narrow resonance located far from all relevant thresholds. In this case, one may use the constant-width Breit-Wigner parameterization,

$$\mathcal{A}(s) = \frac{\tilde{\alpha}}{M_{\mathrm{BW}}^2 - s - i\sqrt{s}\Gamma_{\mathrm{BW}}} \approx \frac{\tilde{\alpha}}{M_{\mathrm{BW}}^2 - s - iM_{\mathrm{BW}}\Gamma_{\mathrm{BW}}} \quad , \tag{49.18}$$

where $\tilde{\alpha}$ contains the resonance coupling to the source as well as to the final state. It is common to replace $\sqrt{s}$ by M_{BW} as done in the right expression.

To use a constant partial width for a resonance coupling to some channel a in an analysis is justified only, if $2(M_{\mathrm{R}} - \sqrt{s_{\mathrm{thr}_a}})/\Gamma_{\mathrm{R}} \gg 1$, where $\sqrt{s_{\mathrm{thr}_a}}$ denotes the location of the threshold for channel a. Otherwise, it is important to build in the appropriate threshold behavior and use the energy-dependent expression for the denominator.

$$\mathcal{A}_a(s) = \frac{\alpha\, g_a\, n_a(s)}{M_{\mathrm{BW}}^2 - s - i\sum_b g_b^2\rho_b(s)n_b^2(s)}, \tag{49.19}$$

where the sum in the denominator is taken over all open channels, n_a combines the threshold and barrier factors, $n_a = (q_a/q_{\mathrm{o}})^{l_a}F_{l_a}(q_a, q_{\mathrm{o}})$, with l_a being the orbital angular momentum in channel a, q_a is given by Eq. (17) of the review on "Kinematics", and q_{o} denotes a mometum scale. The factor $(q_a)^l$ guarantees the correct threshold behavior. The rapid growth of this factor for angular momenta $l > 0$ is commonly compensated at higher energies by a phenomenological form factor, here denoted by $F_{l_a}(q_a, q_{\mathrm{o}})$. Often the Blatt-Weisskopf form factors are used [36–38], where $F_j(q, q_0) = F_j(q/q_0)$ and, *e.g.* $F_0^2(z) = 1$, $F_1^2(z) = 1/(1 + z)$ and $F_2^2(z) = 1/(9 + 3z + z^2)$. The denominator can be written as $M_{\mathrm{BW}}^2 - s - iM_{\mathrm{BW}}\Gamma_{\mathrm{tot}}(s)$, with

$$\Gamma_{\mathrm{tot}}(s) = \sum_b \Gamma_b(s) \tag{49.20}$$

for the energy-dependent total width. An often used parameterization for the partial width $\Gamma_a(s)$ trades the coupling for the resonance width:

$$\Gamma_a(s) = \Gamma_{\mathrm{BW}\,a}\frac{\rho_a(s)}{\rho_a(M_{\mathrm{BW}}^2)}\left(\frac{q_a}{q_{a\,\mathrm{R}}}\right)^{2l_a}\frac{F_{l_a}^2(q_a, q_{\mathrm{o}})}{F_{l_a}^2(q_{a\,\mathrm{R}}, q_{\mathrm{o}})}. \tag{49.21}$$

Here $q_{a\,\mathrm{R}}$ are the values of the break-up momentum evaluated at $s = M_{\mathrm{BW}}^2$. The Breit-Wigner parameters M_{BW} and Γ_{BW} in Eq. (49.18) as well as the coupling g_a in Eq. (49.19) allow for an effective description of resonance phenomena but in general do not have strict physical meaning. The mass and width agree with the pole parameters only if the resonance is narrow in the sense defined above. Otherwise, the Breit-Wigner parameters deviate from the pole parameters and are in general reaction dependent.

Branching fractions for individual, isolated resonances may be introduced based on the parameters introduced above:

$$\mathrm{Br}'_a = \frac{\Gamma_{\mathrm{BW}\,a}}{\Gamma_{\mathrm{BW,tot}}} \tag{49.22}$$

where $\Gamma_{\mathrm{BW,tot}} = \sum_a \Gamma_{\mathrm{BW}\,a}$ denotes the total width evaluated at the Breit-Wigner mass.

The branching fraction definition based on a probability of the decay to a certain channel,

$$\mathrm{Br}''_a = \int\limits_{s_{\mathrm{thr},a}}^{\infty} \mathrm{d}s\, \frac{|g_a|^2\, n_a^2\, \rho_a(s)}{|M_{\mathrm{BW}}^2 - s - iM_{\mathrm{BW}}\Gamma_{\mathrm{tot}}(s)|^2} \left/ \sum_c \int\limits_{s_{\mathrm{thr},c}}^{\infty} \mathrm{d}s\, \frac{|g_c|^2\, n_c^2\, \rho_c(s)}{|M_{\mathrm{BW}}^2 - s - iM_{\mathrm{BW}}\Gamma_{\mathrm{tot}}(s)|^2} \right. , \tag{49.23}$$

is also often used.

If there is more than one resonance in one partial wave that significantly couples to the same channel, it is in general incorrect to use a sum of Breit-Wigner functions, for this usually leads to violation of unitarity constraints. Then, more refined methods should be used, like the K–matrix approximation described in the next section.

49.3.2 K–*matrix approximation and Flatté parameterizations*

The K–matrix method is a general construction for coupled-channel scattering amplitudes $\mathcal{M}_{ba}$ that guarantees two–particle unitarity, but does not allow for the inclusion of left-hand cuts [39]. The amplitude reads,

$$n_b\, \mathcal{M}_{ba}^{-1}\, n_a = \mathcal{K}_{ba}^{-1} - i\delta_{ba}\rho_a n_a^2, \tag{49.24}$$

where $\mathcal{K}_{ba}$ is an arbitrary real function. The factor n_a becomes important for the waves with non-zero angular momentum. As mentioned before $n_a = q_a^{l_a}$ or $n_a = (q_a/q_{\mathrm{o}})^{l_a} F_{l_a}(q_a, q_{\mathrm{o}})$.

As there is no unique rigorous recipe to build $\mathcal{K}$, various parameterizations thereof have to be studied, in order to get access to the theoretical systematic uncertainty. One possible choice for the K–matrix is

$$\mathcal{K}_{ba}(s) = \sum_R \frac{g_b^R g_a^R}{M_R^2 - s} + \sum_{i=0}^{N_{\mathrm{b.g.}}} b_{ba}^{(i)} s^i, \tag{49.25}$$

where M_R is referred to as the bare mass of the resonance R, g_a^R is the bare coupling of the resonance R to the channel a and the $b_{ba}^{(i)}$ are matrices parameterizing the non-pole parts of the K-matrix. As long as all parameters appearing in Eq. (49.25) are real the amplitude is unitary. From the ansatz given above the scattering amplitude $\mathcal{M}$ can be calculated directly using the matrix form,

$$\mathcal{M} = n[1 - \mathcal{K}\, i\rho\, n^2]^{-1}\mathcal{K}\, n \,. \tag{49.26}$$

This solution also applies in those cases in which the inverse of $\mathcal{K}$ does not exist.

As an alternative to Eq. (49.25), the same functional form as on the right side of Eq. (49.25) can be used to parameterize the inverse K–matrix, called by authors of Ref. [40] the M–matrix. The K–matrix framework is extensively used to parameterize the scattering amplitudes needed to analyse the data from lattice QCD calculations [41–43]

One notices that the evaluation of the K–matrix amplitude for the multichannel problem requires an analytic continuation already on the real axis. For a given closed channel c (the channel c is called closed, if $s < s_{\mathrm{thr},c}$), the factor $q_c(s)$ that enters ρ_c and n_c has to be calculated below the corresponding threshold, *i.e.* in the unphysical region of the particular channel c. This is done using analytic continuation as described *e.g.* in Refs. [44, 45]:

$$q_c = i\sqrt{-q_c^2} \quad \text{for} \quad q_c^2 < 0. \tag{49.27}$$

The resulting line shape above and below the threshold of channel c is called the Flatté parameterization [44]. The contiuation given above stays on the physical sheet. To reach the unphysical sheet the negative square root needs to be chosen. If the coupling of a resonance to the channel opening nearby is very strong, the Flatté parameterization shows a scaling invariance and does not allow for an extraction of individual partial decay widths, but only of ratios [46]. The position of the resonance poles can be determined by a study of the zeros of the analytic function $\det[1 - \mathcal{K} i\rho n^2]$. Due to the ρ factor, this determinant has a complicated multisheet structure, however, the closest unphysical sheet is always the one which is determined by the heaviest threshold below the studied point s.

49.3.3 *Scattering-length approximation*

A scattering length, a, is introduced as the first term in an expansion of the scattering phase shift introduced in Eq. (49.10). For S-waves one finds

$$q \cot \delta = 1/a + O(q^2) \,, \tag{49.28}$$

where q is a break-up momentum of the scattering system. In this approximation, the scattering amplitude reads

$$\mathcal{M}(s) = \frac{8\pi\sqrt{s}}{1/a - iq(s)} \,. \tag{49.29}$$

The scattering length is proportional to the value of the amplitude at threshold. The sign of the scattering length is a matter of convention — notably in nuclear physics a sign convention different from Eq. (49.28) is common. A scattering length approximation is applicable only in a very limited energy range, however, might well be appropriate to analyse the recently discovered narrow near-threshold states [47, 48] from this point of view, e.g., in Refs. [49–51]. Moreover, it is possible to introduce the effect of a weakly coupled lower channel. To see this one might start from

$$\mathcal{K} = \begin{pmatrix} \gamma & \beta \\ \beta & 0 \end{pmatrix} \,, \tag{49.30}$$

with β, γ being real numbers. It leads to

$$\mathcal{M}_{\mathrm{el.}}(s) = \frac{1}{1/(\gamma + i\beta^2 \rho_{\mathrm{inel.}}(s)) - i\rho(s)} \,, \tag{49.31}$$

with $\rho_{\mathrm{inel.}}(s)$ being the phase-space factor of the inelastic channel. The scattering length for the amplitude in Eq. (49.31) obtains an imaginary part due to the coupling to the lower channel,

$$a = \frac{1}{8\pi\sqrt{s_{\mathrm{thr}}}} \left(\gamma + i\beta^2 \rho_{\mathrm{inel.}}(s_{\mathrm{thr}}) \right) \,. \tag{49.32}$$

If the function $\beta^2 \rho_{\mathrm{inel.}}(s)$ does not vary significantly in the energy range studied, the scattering length approximation with a complex value is justified. For large values of a the amplitude of Eq. (49.31) develops a near threshold pole located on the physical or unphysical sheet for negative or positive values of γ, respectively. While easy to use, it is important to stress, however, that the approximation in Eq. (49.30) is a specific choice of the dynamic function that produces a single pole near the physical region pointing at a hadronic molecule nature of the state studied [51–53]. For practical analyses, various modifications of the parameterization have to be tested.

49.3.4 *Two methods to build the production amplitude*

When the unitary scattering amplitude is fixed, it can be used to build the production amplitude in a way that it is consistent with unitarity [38, 54].

1. The Q–**vector** approach is discussed in Ref. [38, 40, 55]. It reads,

$$\mathcal{A}_a(s) = \sum_c \mathcal{M}_{ac}(s) Q_c(s)/n_c, \qquad Q_c(s) = \sum Q_c^{(i)} s^i. \qquad (49.33)$$

The unitarity condition of Eq. (49.11) is satisfied when $Q_c(s)$ is a real function and in particular does not have singularities above the lowest threshold for all channels c. Besides these conditions $Q_c(s)$ is arbitrary. Note that in the Q–vector approach the left hand cuts of the scattering matrix $\mathcal{M}_{ac}(s)$ get imported to the production amplitude which might generate a wrong analytic structure. If this problem is relevant needs to be investigated on a case-by-case basis. In a study of $\gamma\gamma \to \pi\pi$, *cf.* Ref. [34, 35] a low-order polynomial is claimed to be sufficient to parametrize the energy dependence of the function $Q_c(s)$. The Q–vector method is convenient, if the full matrix $\mathcal{M}$ is known, *cf.* Ref. [40].

2. The P–**vector** is a parameterization that exploits the K–matrix of the scattering amplitude [39, 54]. It contains two components: the background term B_c that is coupled to the K–matrix via an intermediate loop represented by the $i\rho$ factor, and the "direct" resonance production term with couplings α_c^R:

$$\mathcal{A}_a(s) = n_a \sum_c \left[1 - \mathcal{K} i\rho n^2 \right]^{-1}_{ac} P_c, \qquad P_c = \sum_R \frac{\alpha^R g_c^R}{M_R^2 - s} + B_c. \qquad (49.34)$$

Again, unitarity requires the parameters B_c and α^R to be real. Importantly, the masses M_R need to agree with those in $\mathcal{K}$ in Eq. (49.25).

An important difference between the methods is to be noticed [54]: When the two-particle scattering amplitude goes to zero, the production amplitude in the Q–vector method vanishes for finite values of Q_c, while it stays finite in the P–vector approach. An advanced version of the P–vector approach that exploits analytic properties of production amplitude [54, 56, 57] is widely used, *e.g.* in the dispersive Khuri-Treiman framework [25, 58] for construction of three-body-decay amplitude.

49.3.5 *Further improvements: Chew-Mandelstam function*

The K–matrix described above usually allows one to get a proper fit of physical amplitudes and it is easy to deal with, however, it also has an important deficit: it violates constraints from analyticity — *e.g.*, ρ_a, given by Eq. (49.8), is ill-defined at $s = 0$, and for unequal masses it develops an unphysical cut (see Fig. 49.3). A method to improve the analytic properties was suggested in Refs. [59–63]. It replaces the phase-space factor $i\rho_a(s)$ in Eq. (49.24) by the analytic function $\Sigma_a(s)$ that produces the identical imaginary part on the right-hand cut. This function is called the Chew-Mandelstam function and for S-waves it reads [56, 61]:

$$\Sigma_a(s) = \frac{1}{16\pi^2} \left[\frac{2q_a}{\sqrt{s}} \log \frac{m_1^2 + m_2^2 - s + 2\sqrt{s}q_a}{2m_1 m_2} - (m_1^2 - m_2^2) \left(\frac{1}{s} - \frac{1}{(m_1 + m_2)^2} \right) \log \frac{m_1}{m_2} \right], \quad (49.35)$$

where m_1 and m_2 are masses of the final-state particles in channel a, $s_{\text{thr}_a} = (m_1 + m_2)^2$. The function along the real axis is plotted on the right pane of Fig. 49.1. For channels with $j > 0$, the threshold behavior has to be incorporated properly. This can be done, e.g., by computing the dispersion integral

$$\Sigma_a(s + i0) = \frac{s - s_{\text{thr}_a}}{\pi} \int_{s_{\text{thr}_a}}^{\infty} \frac{\rho_a(s') n_a^2(s')}{(s' - s_{\text{thr}_a})(s' - s - i0)} \, ds'. \qquad (49.36)$$

A further discussion of the calculation of the Chew-Mandelstam function can be found in Ref. [64].
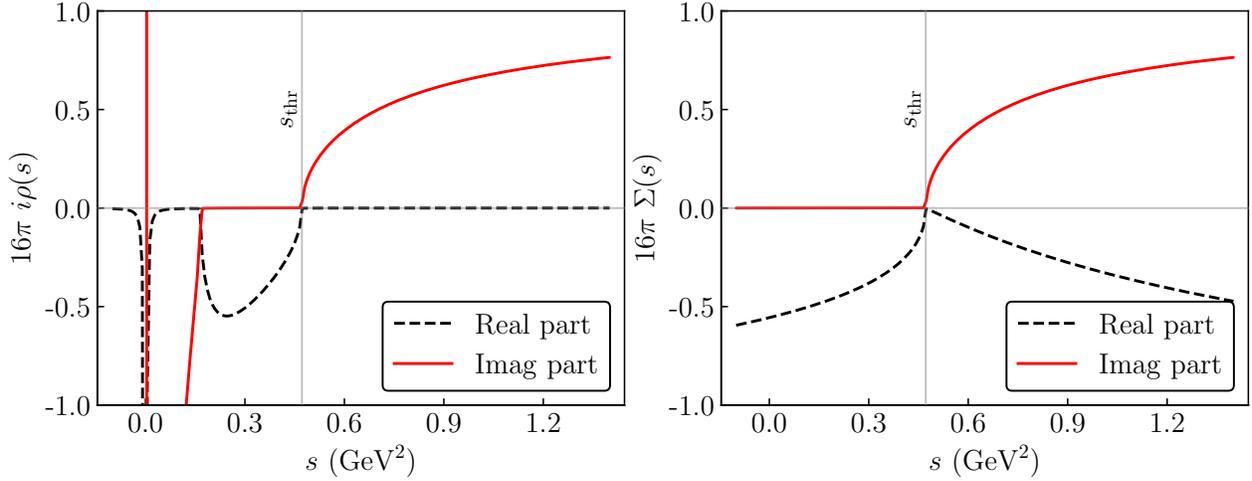

Figure 49.3: Comparison of the $i\rho$ function (left plot) to the Chew-Mandelstam function from Eq. (49.35) (right plot), evaluated for the case of S-wave $\eta\pi$ scattering. The values of s are taken slightly above the real axis, $s + i0$. The solid red line shows the imaginary part that is the same for both functions above threshold. The dashed black line presents the real part. One finds indications of the unphysical left-hand singularities of the function $i\rho$ on the left plot, while the Chew-Mandelstam function in analytic below the two-particle threshold.

If there is only a single resonance in a given channel, it is possible to feed the imaginary part of the Breit-Wigner function, Eq. (49.19) with an energy-dependent width, directly into a dispersion integral to get a resonance propagator with the correct analytic structure [65, 66].

49.3.6 *Two-potential decomposition*

The other advanced technique to construct the scattering amplitude which is widely used in the literature [67–71] is based on the two-potential formalism [72]. The method is usually formulated for the full unprojected amplitude $\mathcal{M}_{ba}(s, t)$, however, in order to simplify the discussion we present the equations in the partial-wave-projected form.

The scattering amplitude $\mathcal{M}$ is decomposed into a pole part and a non–pole part, often called background (b.g.)

$$\mathcal{M}(s) = \mathcal{M}^{\mathrm{b.g.}}(s) + \mathcal{M}^{\mathrm{pole}}(s) \,. \tag{49.37}$$

The splitting given in Eq. (49.37) is not unique and model-dependent (see, *e.g.*, the discussions in Refs. [73, 74]). The background scattering matrix is assumed to be unitary by itself. One option is to parameterize it, e.g. at low energies directly in terms of phase shifts and inelasticities — see, e.g., Refs. [71, 75]. In this case the vertex functions $\Omega(s)_{ab}$ introduced below can be written in terms of an Omnes matrix [75], which reduces to the well known Omnes function in the single channel case [57]. Alternatively, it can be computed based on some potential, $V^{\mathrm{b.g.}}$, fed into a proper scattering equation.

The complete amplitude $\mathcal{M}$ of Eq. (49.37) is unitary if the pole part is chosen as

$$\mathcal{M}^{\mathrm{pole}}(s) = \Omega(s) \left[1 - V^{\mathrm{R}}(s)\Sigma^u(s)\right]^{-1} V^{\mathrm{R}}(s) \; \Omega^T(s) \,. \tag{49.38}$$

where the resonance potential reads in channel space

$$V_{ab}^{\mathrm{R}}(s) = \sum_R \frac{g_a^R \; g_b^R}{M_R^2 - s} \,, \tag{49.39}$$

Σ_{ab}^u denotes the self-energy matrix, and g_a^R and M_R denote the bare coupling of the resonance R to channel a and its bare mass, respectively. A relation analogous to Eq. (49.5) holds for the normalized vertex functions, however, with the final state interaction provided by $\mathcal{M}^{\text{b.g.}}$

$$\text{Disc } \Omega_{ab}(s) = 2i \sum_c \mathcal{M}_{ca}^{\text{b.g.}\,*}(s)\, \rho_c(s)\, \Omega_{cb}(s) \ . \tag{49.40}$$

The discontinuity of the self-energy matrix $\Sigma^u(s)$ is

$$\text{Disc } \Sigma_{ab}^u(s) = 2i \sum_c \Omega_{ca}^*(s)\, \rho_c(s)\, \Omega_{cb}(s) \ . \tag{49.41}$$

The real part of Σ^u can be calculated from Eq. (49.41) via a properly subtracted dispersion integral. If $\mathcal{M}^{\text{b.g.}}$ is unitary, the use of Eq. (49.38) leads to a unitary full amplitude, *cf.* Eq. (49.37). However, the pole term alone is unitary only for a vanishing background amplitude. In this situation the amplitude just described reduces to the analytically improved K-matrix of Sec. 49.3.5. While the omission of non-pole terms is a bad approximation for, *e.g.*, scalar–isoscalar $\pi\pi$ interactions at low energies [76], it typically works well for higher partial waves.

The algebra of the two potential splitting presented in Eq. (49.37) is found to be very practical in various other cases, beyond the pole–background separation. It was employed in Refs. [71, 75] to treat the pion vector and scalar form factor, respectively, over a sizable energy range including inelasticities. A similar decomposition applied to the $3 \to 3$ scattering problem provided a way to isolate the non-separable one-particle exchange singularity from the short-range resonance interaction [77].

Acknowledgement

References

[1] M. Jacob and G. C. Wick, Annals Phys. **7**, 404 (1959), [Annals Phys.281,774(2000)].

[2] C. Zemach, Phys. Rev. **140B**, 97, 109 (1965).

[3] A. V. Anisovich *et al.*, J. Phys. **G28**, 15 (2002), [hep-ph/0105330].

[4] L. Landau, Nucl. Phys. **13**, 181 (1959).

[5] R. Cutkosky, J. Math. Phys. **1**, 429 (1960).

[6] V. N. Gribov, Y. L. Dokshitzer and J. Nyiri, *Strong Interactions of Hadrons at High Energies – Gribov Lectures on Theoretical Physics*, Cambridge University Press, Cambridge (2009).

[7] A rapid change in an amplitude is not an unambiguous signal of a singularity of the S–matrix [78], however, for realistic interactions this connection holds.

[8] S. Coleman and R. E. Norton, Nuovo Cim. **38**, 438 (1965).

[9] C. Schmid, Phys. Rev. **154**, 5, 1363 (1967).

[10] I. J. R. Aitchison and C. Kacser, Il Nuovo Cimento A (1965-1970) **40**, 2, 576 (1965), ISSN 1826-9869, URL https://doi.org/10.1007/BF02721045.

[11] M. Mikhasenko, B. Ketzer and A. Sarantsev, Phys. Rev. **D91**, 9, 094015 (2015), [arXiv:1501.07023].

[12] M. Bayar *et al.*, Phys. Rev. **D94**, 7, 074039 (2016), [arXiv:1609.04133].

[13] F. Aceti, L. R. Dai and E. Oset, Phys. Rev. **D94**, 9, 096015 (2016), [arXiv:1606.06893].

[14] J.-J. Wu *et al.*, Phys. Rev. Lett. **108**, 081803 (2012), [arXiv:1108.3772].

[15] G. Höhler, *Pion-Nucleon Scattering – Methods and Results of Phenomenological Analyses*, Springer-Verlag Berlin, Heidelberg, New York, 1983.

[16] M. Fukugita and K. Igi, Phys. Rept. **31**, 237 (1977).

[17] S. M. Roy, Phys. Lett. **36B**, 353 (1971).

[18] B. Ananthanarayan *et al.*, Phys. Rept. **353**, 207 (2001), [hep-ph/0005297].

[19] G. Colangelo, J. Gasser and H. Leutwyler, Nucl. Phys. **B603**, 125 (2001), [hep-ph/0103088].

[20] R. Garcia-Martin *et al.*, Phys. Rev. **D83**, 074004 (2011), [arXiv:1102.2183].

[21] P. Buettiker, S. Descotes-Genon and B. Moussallam, Eur. Phys. J. **C33**, 409 (2004), [hep-ph/0310283].

[22] M. Hoferichter, D. R. Phillips and C. Schat, Eur. Phys. J. **C71**, 1743 (2011), [arXiv:1106.4147].

[23] M. Hoferichter *et al.*, Phys. Rept. **625**, 1 (2016), [arXiv:1510.06039].

[24] M. P. Peskin and D. V. Schroeder, *An Introduction to Quantum Field Theory*, Westview Press, 1995.

[25] N. N. Khuri and S. B. Treiman, Phys. Rev. **119**, 1115 (1960).

[26] P. Guo *et al.*, Phys. Lett. **B771**, 497 (2017), [arXiv:1608.01447].

[27] M. Albaladejo and B. Moussallam, Eur. Phys. J. **C77**, 8, 508 (2017), [arXiv:1702.04931].

[28] G. Colangelo *et al.*, Eur. Phys. J. **C78**, 11, 947 (2018), [arXiv:1807.11937].

[29] F. Niecknig, B. Kubis and S. P. Schneider, Eur. Phys. J. **C72**, 2014 (2012), [arXiv:1203.2501].

[30] I. V. Danilkin *et al.*, Phys. Rev. **D91**, 9, 094029 (2015), [arXiv:1409.7708].

[31] T. Isken *et al.*, Eur. Phys. J. **C77**, 7, 489 (2017), [arXiv:1705.04339].

[32] F. Niecknig and B. Kubis, JHEP **10**, 142 (2015), [arXiv:1509.03188].

[33] F. Niecknig and B. Kubis, Phys. Lett. **B780**, 471 (2018), [arXiv:1708.00446].

[34] D. Morgan and M. R. Pennington, Z. Phys. **C37**, 431 (1988), [Erratum: Z. Phys.C39,590(1988)].

[35] D. Morgan and M. R. Pennington, Z. Phys. **C48**, 623 (1990).

[36] J. M. Blatt and V. F. Weisskopf, *Theoretical nuclear physics*, Springer, New York (1952), ISBN 9780471080190.

[37] F. Von Hippel and C. Quigg, Phys. Rev. **D5**, 624 (1972).

[38] S. U. Chung *et al.*, Annalen Phys. **4**, 404 (1995).

[39] I. J. R. Aitchison, Nucl. Phys. **A189**, 417 (1972).

[40] K. L. Au, D. Morgan and M. R. Pennington, Phys. Rev. **D35**, 1633 (1987).

[41] J. J. Dudek, R. G. Edwards and D. J. Wilson (Hadron Spectrum), Phys. Rev. **D93**, 9, 094506 (2016), [arXiv:1602.05122].

[42] R. A. Briceno *et al.*, Phys. Rev. **D97**, 5, 054513 (2018), [arXiv:1708.06667].

[43] A. J. Woss *et al.* (2019), [arXiv:1904.04136].

[44] S. M. Flatte, Phys. Lett. **63B**, 224 (1976).

[45] V. V. Anisovich and A. V. Sarantsev, Eur. Phys. J. **A16**, 229 (2003), [hep-ph/0204328].

[46] V. Baru *et al.*, Eur. Phys. J. **A23**, 523 (2005), [arXiv:nucl-th/0410099].

[47] S. K. Choi *et al.* (Belle), Phys. Rev. Lett. **91**, 262001 (2003), [hep-ex/0309032].

[48] R. Aaij *et al.* (LHCb), Phys. Rev. Lett. **122**, 22, 222001 (2019), [arXiv:1904.03947].

[49] E. Braaten and J. Stapleton, Phys. Rev. **D81**, 014019 (2010), [arXiv:0907.3167].

[50] V. Baru *et al.*, Eur. Phys. J. **A44**, 93 (2010), [arXiv:1001.0369].

[51] C. Fernández-Ramírez *et al.* (JPAC), Phys. Rev. Lett. **123**, 9, 092001 (2019), [arXiv:1904.10021].

[52] D. Morgan, Nucl. Phys. **A543**, 632 (1992).

[53] V. Baru *et al.*, Phys. Lett. **B586**, 53 (2004), [hep-ph/0308129].

[54] I. J. R. Aitchison (2015), [arXiv:1507.02697].

[55] R. N. Cahn and P. V. Landshoff, Nucl. Phys. **B266**, 451 (1986).

[56] J. L. Basdevant and E. L. Berger, Phys. Rev. **D16**, 657 (1977).

[57] R. Omnes, Nuovo Cim. **8**, 316 (1958).

[58] I. J. R. Aitchison and R. Pasquier, Phys. Rev. **152**, 4, 1274 (1966).

[59] G. J. Gounaris and J. J. Sakurai, Phys. Rev. Lett. **21**, 244 (1968).

[60] M. R. Pennington *et al.*, Eur. Phys. J. **C56**, 1 (2008), [arXiv:0803.3389].

[61] J. A. Oller and E. Oset, Phys. Rev. **D60**, 074023 (1999), [hep-ph/9809337].

[62] N. N. Achasov and A. V. Kiselev, Phys. Rev. **D83**, 054008 (2011), [arXiv:1011.4446].

[63] A. V. Anisovich *et al.*, Phys. Rev. **D84**, 076001 (2011).

[64] J. H. Reid and N. N. Trofimenkoff, J. Math. Phys. **25**, 3540 (1984).

[65] E. L. Lomon and S. Pacetti, Phys. Rev. **D85**, 113004 (2012), [Erratum: Phys. Rev.D86,039901(2012)], [arXiv:1201.6126].

[66] B. Moussallam, Eur. Phys. J. **C73**, 2539 (2013), [arXiv:1305.3143].

[67] I. R. Afnan and B. Blankleider, Phys. Rev. **C22**, 1638 (1980).

[68] A. D. Lahiff and I. R. Afnan, Phys. Rev. **C60**, 024608 (1999), [arXiv:nucl-th/9903058].

[69] A. Matsuyama, T. Sato and T. S. H. Lee, Phys. Rept. **439**, 193 (2007), [arXiv:nucl-th/0608051].

[70] D. Ronchen *et al.*, Eur. Phys. J. **A49**, 44 (2013), [arXiv:1211.6998].

[71] C. Hanhart, Phys. Lett. **B715**, 170 (2012), [arXiv:1203.6839].

[72] K. Nakano, Phys. Rev. **C26**, 1123 (1982).

[73] D. Djukanovic, J. Gegelia and S. Scherer, Phys. Rev. **D76**, 037501 (2007), [arXiv:0707.2030].

[74] M. Doring *et al.*, Phys. Lett. **B681**, 26 (2009), [arXiv:0903.1781].

[75] S. Ropertz, C. Hanhart and B. Kubis, Eur. Phys. J. **C78**, 12, 1000 (2018), [arXiv:1809.06867].

[76] J. Gasser and U. G. Meissner, Nucl. Phys. **B357**, 90 (1991).

[77] M. Mikhasenko *et al.*, JHEP **08**, 080 (2019), [arXiv:1904.11894].

[78] G. Calucci, L. Fonda and G. C. Ghirardi, Phys. Rev. **166**, 1719 (1968).